EXPERIMENTAL CLAY-MINERAL FORMATION FROM A SUBVOLCANIC ROCK BY INTERACTION WITH 1 M NaOH SOLUTION AT ROOM TEMPERATURE

A. Drief, F. Nieto, and A. Sanchez-Navas

Departamento de Mineralogía y Petrología, Instituto Andaluz de Ciencias de la Tierra, Universidad de Granada-C.S.I.C, Av. Fuentenueva s/n, 18002 Granada, Spain

Abstract—The alteration process of a subvolcanic rock with calcic plagioclase, pyroxene, and olivine as major components was investigated by X-ray diffraction (XRD) and analytical and transmission electron microscopy (TEM/AEM). Experimental interaction with 1 M NaOH solution led to the formation of dioctahedral beidellite to Fe-rich montmorillonite after 1 and 3 d of reaction. This range of smectite composition is similar to that from natural subvolcanic-derived soil formed from the same parent material. After 14 d of reaction, a berthierine-smectite (B-S) interstratified clay had partially replaced the smectite. Although, the presence of smectite interlayers prevented analysis of pure berthierine, berthierine-rich B-S interstratifications have a composition similar to pure berthierine. After 40 d, the alteration process led to a 7-Å S interstratification whose composition falls between greenalite and lizardite. A series of amorphous materials were also found in the 14 and 40-d experiments. The most abundant of these is a Si-Ca-Fe-rich material, whose chemical composition approaches that of the starting rock. In contrast, two other amorphous materials had a smectitic composition.

Key Words—AEM Analysis, Berthierine, Interstratification, Lizardite, NaOH Solution, Smectite.

INTRODUCTION

Clay minerals such as smectites are widely distributed over the earth's crust as the weathering products of volcanic glasses or rock-forming minerals. Smectites have been synthesized at low temperature using various starting materials. Farmer *et al.* (1991a, 1991b) found that saponite- and nontronite-like structures developed from aluminosilicate precipitates digested in solutions containing Mg and Fe ions, respectively. Plee *et al.* (1987) and Schultz *et al.* (1987) reported the synthesis of beidellite from aluminosilicate gel in NaOH solutions at 300–340°C. Grauby *et al.* (1993) synthesized smectite in the beidellite-saponite series using synthetic gels at 200°C. On the basis of transmission electron microscopy (TEM) analysis, they concluded that the Al-Mg series was continuous between beidellite and montmorillonite end-members. The formation of beidellite using aluminosilicate gel as starting material was also investigated by Kloprogge *et al.* (1990), with experiments performed in NaOH solutions with pH ranging from 7.5 to 13.5 at a temperature of 350°C. According to these authors, the most highly crystallized beidellite was obtained at 350°C, 1 Kbar, 5 d of reaction, and a pH of 10 in the starting solution. Kawano and Tomita (1992) reported the formation of beidellite by hydrothermal alteration of volcanic glass below 200°C. More recently, the same authors (Kawano and Tomita, 1994) studied the growth of smectite from leached layers during the experimental alteration of albite in deionized-distilled water at temperatures ranging from 150 to 225°C.

Berthierine, less common in nature than smectite, is an iron-rich aluminous trioctahedral 1:1-type phyllos-

ilicate belonging to the serpentine-kaolin group (Bailey, 1980). This layer silicate has been previously refered to as "septechlorite", "septechamosite", chamosite, aluminous lizardite, and "7-Å chlorite". Berthierine is chemically similar to chamosite, the iron-rich chlorite end-member. The chemical formula of berthierine, as proposed by Brindley (1982), is $(R^{2+}, R^{3+}, \square)_3 (Si_{2-x}Al_x)O_5(OH)_4$, where R^{2+} consists of Fe^{2+}, Mg^{2+}, and Mn^{2+}; R^{3+} comprises Fe^{3+} and Al^{3+} in octahedral sites, and $\square$ represents possible vacant octahedral sites.

Berthierine is not easy to distinguish from Fe-rich chlorites because of the overlap of many of their X-ray diffraction (XRD) lines. For example, Fe-rich chlorite has very intense even basal ($00l$, l = even) X-ray reflections and therefore may be very similar to a mixture of clinochlore and berthierine. Berthierine also shares similarities with kaolinite, a dioctahedral member of the serpentine-kaolin group.

Berthierine commonly occurs in marine sediments, especially in marine oolitic ironstone formations (*e.g.*, Bhattacharyya, 1983). It usually derives from marine rocks or from rocks influenced by marine waters during early diagenesis (Hallam and Bradshaw, 1979). However, non-marine occurrences have also been described. Taylor (1990), for instance, reported a berthierine from non-marine Wealden (Early Cretaceous) sediments in southeast England. He described an intraformational conglomerate containing pisoids and pseudo-ooids with a quartz-siderite-berthierine mineral assemblage deposited in a fresh-to-brackish-water mudplain. Toth and Fritz (1997) described an Fe-rich

Table 1. EMPA analyses and structural formulae of the major minerals of the starting material.

Oxides	Clinopyroxene		Olivine		Plagioclase					
	1	2	1	2	1	2	3	4	5	6
SiO_2	49.75	49.73	36.37	36.44	49.58	49.92	48.13	51.39	63.08	67.55
Al_2O_3	3.16	3.34	0.01	0.00	31.59	31.59	32.73	30.50	23.65	20.32
MgO	13.35	13.27	31.43	31.54	0.02	0.03	0.02	0.03	0.39	0.00
FeO	8.11	8.23	30.99	30.80	0.33	0.31	0.31	0.31	0.40	0.04
CaO	21.10	20.92	0.31	0.30	14.40	14.43	15.69	13.30	3.87	0.70
Na_2O	0.38	0.42	0.02	0.01	3.11	3.18	2.44	3.77	8.43	1.14
TiO_2	2.00	2.11	0.03	0.03	0.07	0.07	0.06	0.10	0.05	0.00
K_2O	0.00	0.02	0.00	0.01	0.17	0.18	0.12	0.25	1.23	0.28
MnO	0.19	0.16	0.42	0.46	0.00	0.00	0.01	0.00	0.01	0.00
Total	98.04	98.23	99.66	99.69	99.26	99.71	99.52	99.64	101.11	100.03
				Structural formulae						
Si	1.89	1.89	2.00	2.00	2.28	2.29	2.22	2.35	2.77	2.95
^{IV}Al	0.11	0.11	0.00	0.00	1.72	1.71	1.78	1.65	1.23	1.05
^{VI}Al	0.03	0.04	0.00	0.00						
Mg	0.76	0.75	2.57	2.58						
Ti	0.06	0.06	0.00	0.00						
Fe	0.26	0.26	1.42	1.41	0.01	0.01	0.01	0.01	0.01	0.00
Mn	0.01	0.01	0.02	0.02						
Na	0.03	0.03	0.00	0.00	0.28	0.28	0.22	0.33	0.72	0.94
Ca	0.86	0.85	0.02	0.02	0.71	0.71	0.78	0.65	0.18	0.03
K	0.00	0.00	0.00	0.00	0.01	0.01	0.01	0.01	0.07	0.02
Σ oct. cat.	2.00	2.00	4.03	4.03						
Σ (Na, K, Ca)	0.89	0.88	0.02	0.02	1.00	1.00	1.00	1.00	0.97	0.99
O	6.01	6.01	8.02	8.01	8.02	8.02	8.02	8.02	8.01	7.99

berthierine from a Cretaceous laterite whose formation occurred in an exclusively non-marine depositional environment.

Berthierine is considered to be a precursor of chlorite during diagenesis (e.g., Longstaffe et al., 1992) and, in fact, chlorite-berthierine intergrowths were described by Jiang et al. (1992). In these assemblages of apparent hydrothermal origin, berthierine is thought to have formed as a replacement for chlorite under non-equilibrium, retrograde conditions. Other authors have reported the same kind of intercalation (Lee and Peacor, 1983; Ahn and Peacor, 1985; Amouric et al., 1988; Jahren and Aagaard, 1989; Hillier and Velde, 1992).

Because most syntheses of smectite were performed using synthetic starting materials under hydrothermal conditions, the aim of the present study is to understand the formation of clay minerals from a subvolcanic rock during its interaction with 1 M NaOH solution at room temperature. Clearly such a high pH solution is not usual in natural conditions, but the use of this pH was necessary to accelerate the reaction process. We used smectite from the subvolcanic-derived soil to compare experimental conditions with natural ones. The use of high-resolution transmission electron microscopy and analytical electron microscopy (HRTEM/AEM) was indispensable to characterize the different phases generated during the alteration process, their chemical compositions, and their textural relationships. Interstratifications of berthierine-smectite (hereafter B-S) and ferroan lizardite-smectite (hereafter Fe-rich L-S) not previously reported are described.

MATERIAL AND EXPERIMENTAL METHODS

Material

Geological setting. Experimental alteration was performed using a subvolcanic rock from the External Zone of the Betic Cordilleras, near the locality of Alcalá La Real, southern Spain. The intrusive subvolcanic rock is emplaced in Triassic sedimentary units (Trias Keuper), mostly preserved as small tectonic blocks, and usually termed *ophites* in the regional bibliographic references (e.g., Portugal-Ferreira et al., 1995). The outcrop of the subvolcanic rock has been exposed in an abandoned quarry for more than twenty years. The subvolcanic-derived soil, hereafter VS, was studied by Drief and Nieto (2000). The material was used for further comparison with the alteration products found in the present study. Because the occurrence of the soil is topographically free from other influences, the subvolcanic rock is the only source material for the soil. Moreover, the phases, as determined by X-ray diffraction and TEM/AEM, show an assemblage similar to the parent rock, but with a significant amount of smectite and lacking 7-Å clay minerals (Drief and Nieto, 2000).

Petrography. Morata et al. (1997) distinguished two groups among the *ophites* on the basis of petrographic characteristics. The group to which our subvolcanic rock belongs is characterized by the presence of olivine. Calcic plagioclase and pinkish Ti-rich augite have an ophitic texture. Ti-rich amphibole and biotite are accessory minerals, together with apatite and Fe-
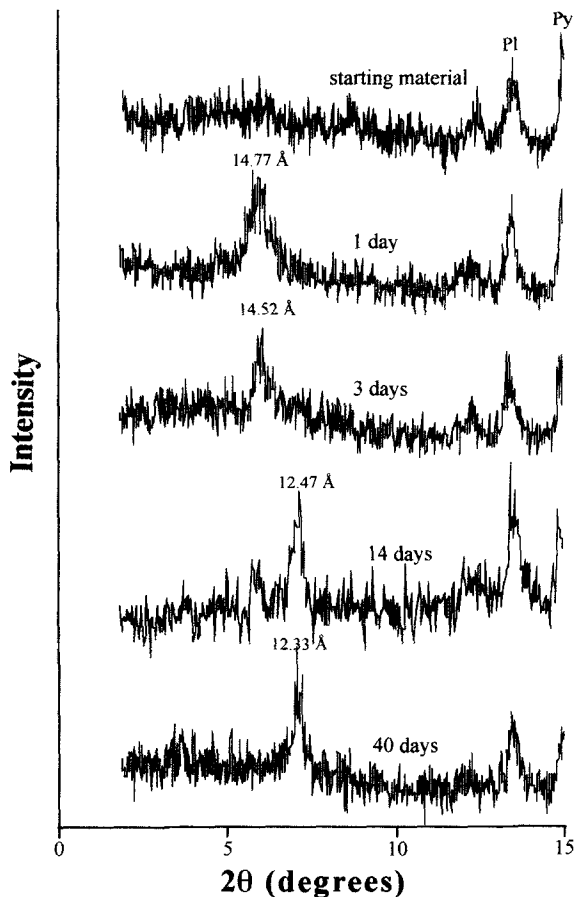
Figure 1. X-ray diffraction patterns of air-dried reaction products formed during experimental alteration of subvolcanic rock with 1 M NaOH solution. Pl = plagioclase and Py = pyroxene.

Ti ores. Quartz is absent. We have studied the starting rock by TEM/AEM to be certain that the rock does not contain clay minerals.

Geochemistry. The whole-rock chemistry of the starting material determined by X-ray fluorescence (XRF) was (in wt. %): 49.35, SiO_2; 19.42, Al_2O_3; 8.20, Fe_2O_3; 4.73, MgO; 0.11, MnO; 9.46, CaO; 4.13, Na_2O; 0.73, K_2O; 1.30, TiO_2; and 0.20, P_2O_5. The loss on ignition (L.O.I.) is 1.66 wt. %. Electron microprobe analysis (EMPA) data of the major minerals are listed in Table 1.

Treatment of the material with 1 M NaOH solution

The subvolcanic rock was gently ground in an agate mortar. The specific surface area obtained was 3.16 m^2/g. An amount of 3 g of the sample was placed in a glass flask with 500 mL of 1 M NaOH solution at room temperature for 1, 3, 14, and 40 d. After each reaction period, solids and solutions were separated. The residual material was then cleaned by distilled-deionized water to remove adhering salts.

Examination of the material

X-ray diffraction. The starting material and the whole residual solid fraction after each experiment time were smeared on glass slides and allowed to dry under atmospheric conditions. Three slides for each experiment were prepared for further X-ray analysis. One of them was saturated with ethylene glycol at 80°C for 24 h to ensure maximum saturation and another was heated at 550°C for 1 h. X-ray diffractograms were obtained using a Philips PW-1710 diffractometer (with graphite monochromater and automated slit) operating at 40 kV and 40 mA, with a scanning speed of 2 °2θ/ min using CuKα radiation.

Electron microscopy. Transmission electron microscopy was performed with a Philips CM20 instrument equipped with an EDAX solid state ultrathin-window energy dispersive X-ray (EDX) detector ["Centro de Instrumentación Científica" (C.I.C.), Granada University]. A small part of solid produced at 3 and at 40 d of reaction was dispersed in distilled water and then deposited on collodion films coated on copper and gold grids. The samples were air-dried at room temperature. In addition, a small portion of residual solid produced after 14 and after 40 d of reaction was embedded in epoxy resin from which a thin section prepared with Canadian-Balsam was made. Copper rings were attached to selected zones and the corresponding areas were detached by gentle heating and then ion thinned using a Gatan 600 ion mill and carbon coated for TEM observation. Acceleration voltage of the microscope was 200 kV and a lens aperture of 40 μm was used as a compromise between amplitude and phase contrast for the images, so reflections with *d* values >0.4 nm were used for the lattice-fringe images. AEM analyses were obtained only from thin edges in a scanning TEM (STEM) mode (<400 counts/s) using a 4-nm diameter beam and 20 × 100 nm scanning area. A low-background condenser aperture and an analytical Be sample holder were employed to improve spectrum quality. Muscovite, albite, biotite, spessartine, olivine, and titanite were used to obtain *k*-factors to correct X-ray intensities by the thin-film method of Lorimer and Cliff (1976). Average errors for analyzed elements (two standard deviations), expressed as a percentage of the atomic proportions, are 6 (Na), 3 (Mg), 2 (Al), 4 (K), 4 (Ca), 5 (Ti), 3 (Mn), and 3 (Fe). A long counting time (200 s) was used because no alkali loss was observed during the analysis. Iron was assumed to be in ferric form for smectite (Drief and Nieto, 2000) and in ferrous form for berthierine and ferroan lizardite as is usual for the sepentine group (*e.g.,* Abad-Ortega and Nieto, 1995; Guggenheim *et al.,* 1982).

RESULTS

X-ray study

The X-ray diffraction patterns of the material treated for 1 d showed a 14–15-Å peak (Figure 1). This phase
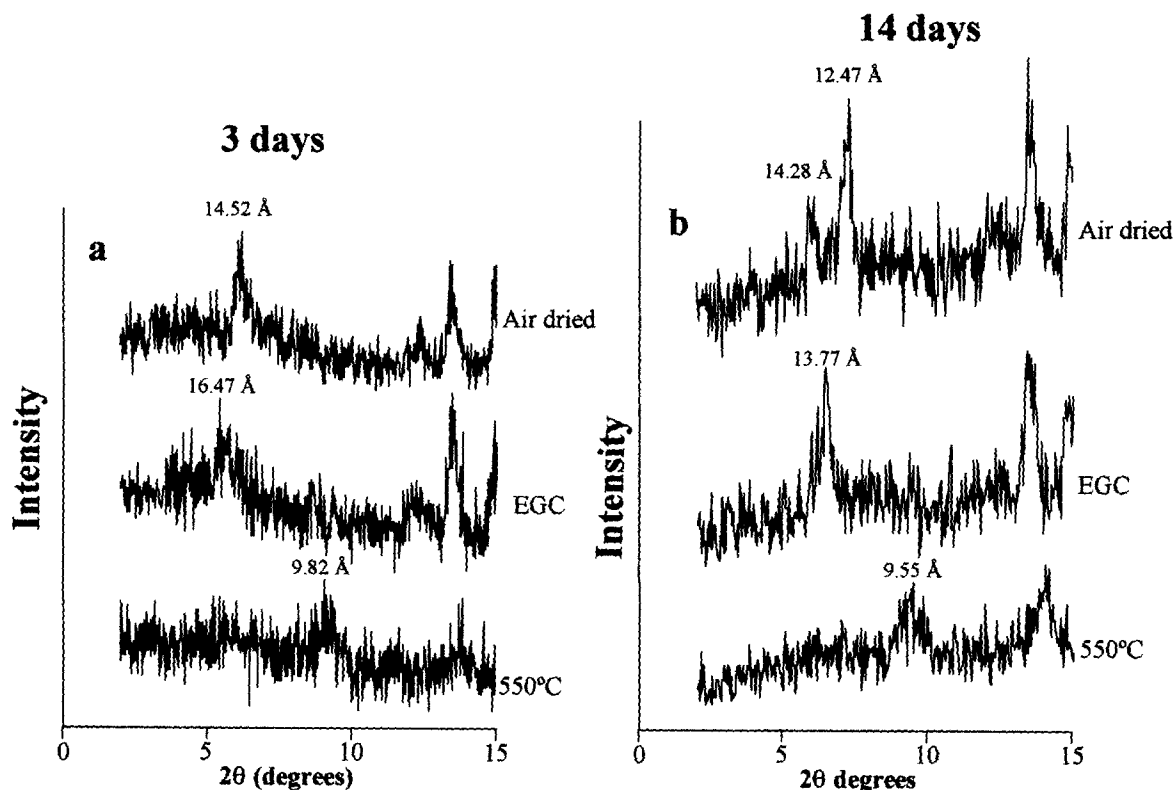
Figure 2. X-ray diffraction patterns of the oriented samples corresponding to (a) 3-d and (b) 14-d reaction products. EGC = glycolated sample, and 550°C = heated to 550°C.

was expanded to 16–17 Å by treatment with ethylene glycol and collapsed by heating to 10 Å (not shown). The same patterns were observed for the 3-d reaction (Figures 1 and 2a). This behavior is similar to that of natural smectites. At 14 d, a new phase precipitated. The X-ray pattern of this phase shows a peak at 12.47 Å (Figures 1 and 2b), which expanded to 13.77 Å after treatment with ethylene glycol (Figure 2b). When heated, this phase was partially destroyed and collapsed to 9.55 Å. Another peak at 14.28 Å shows the partial persistence of smectite at 14 d of reaction. The same patterns occur after 40 d (not shown).

Transmission electron microscopy

Reaction products after three days. After 3 d of reaction, only smectite had formed. The structural formulae of this smectite based on AEM analyses (on the basis of 11 oxygen atoms), along with that of the smectite from the soil derived from the subvolcanic rock, are listed in Table 2. These formulae show that both Si and Al contents range widely. Silica varies between 3.23–3.98 per formula unit (pfu) whereas Al ranges from 2.16 to 1.44 pfu. The ranges in which Mg and Fe vary are wide as well, suggesting that different varieties of smectites are present. The Fe content is, in general, higher than that of Mg. These analyses

showed a very heterogeneous interlayer composition with regard to the interlayer cations.

A plot of the octahedral composition of the reaction after 3 d and VS smectites in an AlMg-AlAl-AlFe ternary system (Güven, 1988) showed that the 3-d reaction products and VS smectite compositions do not fall within a single field assigned to a particular species of dioctahedral smectite, but to fields characteristic of beidellite to Fe-rich montmorillonite (Figure 3). The VS and the reaction smectites have similar dioctahedral compositions. However, their composition begins to diverge as they approach the AlMg-AlFe side of the plot: the reaction smectite composition is richer in Fe, whereas that of the VS smectite is richer in Mg. Generally, the scattering of the analyses for both samples ranges between beidellite and Fe-rich montmorillonite.

The substitution of ^{VI}Al by Fe in the octahedral sites varies widely, providing a well-defined negative relationship (Figure 4a), which is better defined for the reaction smectite (R = 0.96) than the VS smectite. A similar negative relationship is also observed between ^{VI}Al and Mg (Figure 4b), although it is better defined for the VS smectite. No significant relationship was found between Si and Mg or between Fe and Si (not shown). Nevertheless, there is a poorly defined positive relationship between Fe and Mg (Figure 4c). Fi-

Table 2. AEM data for the 3-d reaction product and VS smectites using both copper and gold grids. Analyses were normalized for 10 O and 2 (OH).

	Si	^{IV}Al	^{VI}Al	Mg	Fe	Σ oct. cat.	K	Ca	Na	Σ Int. Cha.
					Structural formulae of the smectite formed at 3 d of reaction					
					Copper grids analyses					
1	3.58	0.42	1.38	0.22	0.49	2.09	0.18	0.09	0.00	0.36
2	3.61	0.39	1.16	0.25	0.69	2.10	0.09	0.10	0.00	0.29
3	3.79	0.21	1.41	0.09	0.49	1.99	0.10	0.08	0.00	0.26
4	3.74	0.26	1.18	0.20	0.61	1.99	0.09	0.17	0.00	0.43
5	3.64	0.36	1.80	0.13	0.14	2.07	0.00	0.12	0.00	0.24
6	3.56	0.44	1.14	0.18	0.73	2.05	0.04	0.18	0.00	0.40
					Gold grids analyses					
7	3.88	0.12	1.68	0.12	0.21	2.01	0.00	0.02	0.10	0.14
8	3.98	0.02	1.71	0.12	0.04	1.93	0.00	0.00	0.38	0.38
9	3.23	0.77	0.91	0.42	0.76	2.09	0.00	0.10	0.16	0.36
10	3.53	0.47	1.54	0.15	0.32	2.01	0.00	0.27	0.00	0.54
				Structural formulae of the smectite of the subvolcanic-derived soil (from Drief and Nieto, 2000)						
					Copper grids analyses					
1	3.23	0.77	1.44	0.26	0.47	2.17	0.25	0.10	0.00	0.45
2	3.86	0.14	1.27	0.39	0.39	2.05	0.07	0.13	0.00	0.33
3	3.73	0.22	1.78	0.15	0.19	2.12	0.02	0.07	0.00	0.16
4	3.81	0.19	1.28	0.52	0.34	2.14	0.04	0.11	0.00	0.26
5	3.74	0.26	1.27	0.39	0.49	2.15	0.04	0.06	0.00	0.16
6	3.70	0.30	1.30	0.34	0.44	2.08	0.04	0.17	0.00	0.38
7	3.44	0.56	1.72	0.18	0.23	2.13	0.11	0.08	0.00	0.27
8	3.69	0.31	1.36	0.32	0.42	2.10	0.09	0.10	0.00	0.29
9	3.69	0.21	1.67	0.21	0.29	2.17	0.10	0.08	0.00	0.26
10	3.43	0.57	1.33	0.36	0.49	2.18	0.18	0.09	0.00	0.36
11	3.62	0.38	1.09	0.61	0.49	2.19	0.12	0.15	0.00	0.42
					Gold grids analyses					
12	3.27	0.73	1.63	0.22	0.24	2.10	0.03	0.21	0.23	0.69
13	3.11	0.89	0.94	0.22	1.07	2.24	0.01	0.12	0.16	0.40
14	3.16	0.84	1.84	0.19	0.11	2.13	0.06	0.16	0.25	0.63
15	3.84	0.16	1.10	0.35	0.54	1.99	0.08	0.06	0.10	0.29

nally, there is a weakly defined negative relationship between Al and Si for the VS smectite that is absent for the reaction smectite (Figure 4d).

Reaction products after fourteen days. At 14 d of reaction, TEM images show smectite layers with ~1-nm spacing (Figure 5a), curved at the edges of the packets. A berthierine-smectite interstratification was found also (Figure 5b). The structural formulae of B-S, calculated from AEM analyses performed on B-S packets are listed in Table 3. X-ray results show that, on the whole, smectite layers are more abundant than berthierine layers in the B-S interstratifications. However, the analyses in Table 3 were performed in berthierine-rich areas to characterize the chemical composition of berthierine and then normalized to 10 O and 8 (OH) assuming that Fe was in ferrous form. In Table 3, Ca and K, which cannot enter the octahedral sites of berthierine, indicate smectite layers intergrown with berthierine. Ca is the dominant interlayer cation of smectite interstratified with berthierine at 14 d of reaction. Although some analyses showed a small amount of K, this cation is generally absent. Tetrahedral and octa-

hedral cations of B-S are plotted in Figure 6. B-S interstratifications showed that ^{VI}Al varies widely (0.56–1.36), whereas Fe remains approximately constant (Figure 6a). This was not the case for Mg *vs.* ^{VI}Al, where a generally negative relationship is observed (Figure 6b). A positive relationship between Si and octahedral Al is well defined in Figure 6f. A poor negative relationship between ^{VI}Al and ^{IV}Al is also observed in Figure 6c. These changes in the composition of B-S are attributed to the number of smectite layers intergrown in the berthierine packets rather than to the berthierine layers. The analyses in Table 3 show the common characteristics of chlorite minerals contaminated by dioctahedral phases, such as high Si, low octahedral-cation sums, and the presence of large cations common to interlayer sites.

TEM images also revealed the presence of amorphous material intimately intergrown with smectite particles. Spindle-like smectite packets that have detached from the edges of plagioclase (Figure 7a) occur with an amorphous Fe-rich material (Figure 7b), as shown by chemical analyses of these areas. Fe-rich
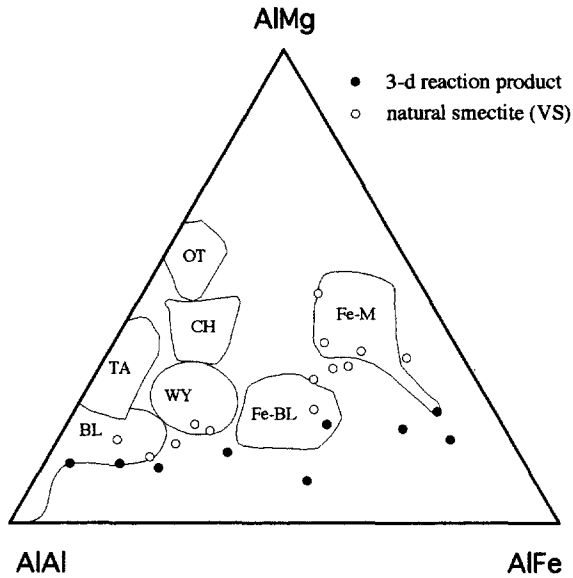
Figure 3.   Projection of the octahedral composition of both 3-d reaction product and VS natural-soil smectites in the ternary system AlMg-AlAl-AlFe as proposed by Güven (1988). OT = Otay montmorillonite, CH = Chambers montmorillonite, TA = Tatatilla montmorillonite, WY = Wyoming montmorillonite, BL = Beidellite, Fe-BL = Fe-rich beidellite, Fe-M = Fe-rich montmorillonite. AEM analyses are those of Table 2.

amorphous material was sometimes found included within smectite packets (Figure 8). Fe-, Si-, and Ca-rich amorphous substances appear associated with smectite particles forming ovoidal to ellipsoidal structures with sizes of between 25–50 nm in diameter (A in Figure 9a and 9b). Another feature of these spherical structures is that they constitute aggregates of mostly electron-dense spheres from 2 to 10 nm in diameter (Figure 9b and 9c). Two other types of non-crystalline substances appear intimately associated with this amorphous material and the smectites. One consists of hollow spheres with more electron-dense walls than centers (A″ in Figure 9c). The second shows fringe contrast and morphologies similar to strongly curved clay-precursor particles (A′ in Figure 9c). Better contrast was not possible despite tilting the sample. Chemical analyses (not shown) of the two kinds of amorphous material (A′ and A″) reveal compositions similar to that of the adjacent smectite.

Reaction products after 40 days. Reaction products are similar to those found after reactions were inspected after 14 d, with all the same phases present. Randomly stratified 0.7- and 10-nm packets were observed (Figure 10). Figure 10 also shows a two-layer stacking sequence with a spacing of 1.4 nm. Unlike the 14-d sample, the AEM analyses (Table 4; Figure 6) showed this sequence to be ferroan lizardite and smectite interstratifications. The plot of octahedral and tetrahedral

cations in Figure 6 depicts the same characteristics as the B-S after 14 d. In both cases, the scatter of points is related to smectite content. However, it can be inferred that the B-S present after 14 d and the Fe-rich L-S interstratification are two distinct phases; the plots of the tetrahedral and octahedral compositions fall within different compositional areas. The values for the Mg, Si, and Al contents are quite different; the quasi-saturation of the tetrahedral sheet by Si led to a decrease in Al in both the tetrahedral and octahedral sites. The Mg content after 40 d is greater than after 14 d: the loss of Al from the octahedral sheet allowed the incorporation of Mg from solution to form a Mg-rich interstratification, with Fe remaining constant. The interlayer composition was dominated by Ca. B-S and Fe-rich L-S interstratifications are related by the Tschermak exchange vector $Si + Mg \rightarrow {}^{IV}Al + {}^{VI}Al$.

Amorphous materials found after 40 d are similar to those found in the 14-d experiment. These materials increased in size in relation to those present after 14 d. These particles are 200 nm in diameter and contain rounded 20-nm electron-translucent centers, probably the result of volatiles released when damaged by the electron beam. The presence of an oxygen peak and rounded areas with light contrast (Figure 11) produced by its dehydration during observation under TEM indicates that the Si-Ca-Fe-rich amorphous material is an oxyhydroxide.

DISCUSSION AND CONCLUSIONS

The general sequence of events observed during the alteration process of subvolcanic rock by interaction with 1 M NaOH solution at room temperature includes: 1) the precipitation of dioctahedral smectite, with a chemical composition similar to that of smectite formed under natural conditions (VS); 2) berthierine-smectite interstratifications with various amorphous materials; and 3) Fe-rich lizardite-smectite interstratifications, found after 40 days.

Smectite formation

The structural formulae of smectite formed after 3 d of reaction are similar to those of VS smectite except for the Fe/Mg ratio, which is higher in the former. A low interlayer charge is observed after 3-d smectite, as well as in the VS smectites. In fact, the assumption that Mg only occupies octahedral sites results in an overestimation of the amount of octahedral cations and an underestimation of the interlayer charge. Most smectites contain >2 atoms per half unit cell (on the basis of 10 O), indicating the possible presence of Mg in the interlayer sites. Christidis (1989) found that in the Garyfalakena deposits, Mg occupies ~70% of the exchangeable sites. Also, Schiffman and Southard (1996) measured the cation-exchange capacity and extractable cations of smectite with both traditional bulk methods and an *in situ* method using the electron mi-
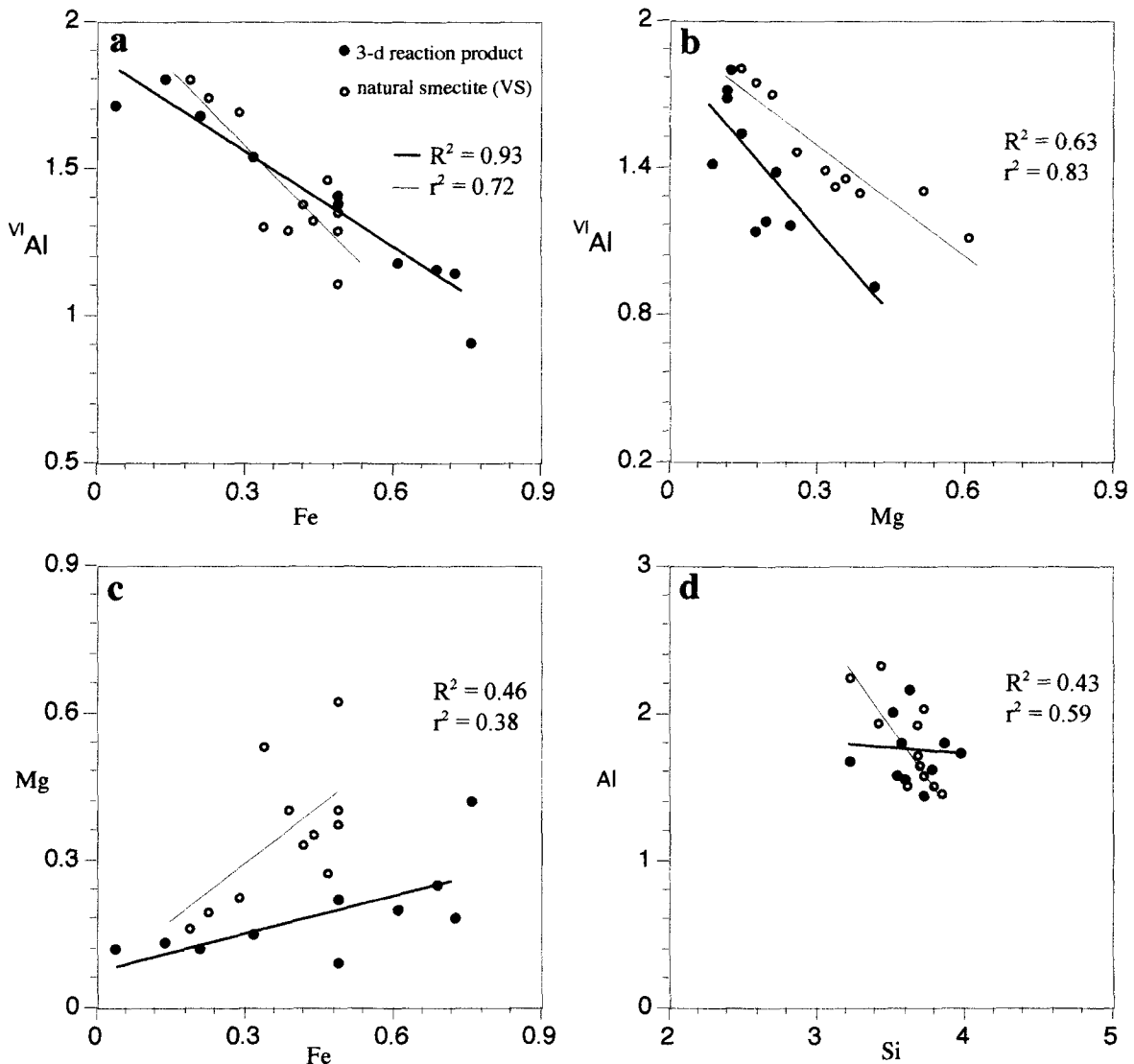
Figure 4. Selected binary diagrams showing the compositional variation in the 3-d reaction product and VS smectites. AEM analyses are those of Tables 2. R^2 and r^2 values correspond to 3-d reaction product and VS smectites, respectively.

croprobe. They found that the *in situ* method implies that Mg is the major extractable cation in this smectite. Owing the overlapping of the L band of Cu and the K band of Na, we also used gold grids to analyze Na and to quantify the interlayer occupancy. When gold grids were used for the 3-d reaction product and the VS smectites (Table 2), a considerable amount of Na was detected. Nonetheless, considerable amounts of Ca were always present. The presence of Na in the interlayer of smectite may be a result of its incorporation from solution and/or from the parent plagioclase. Note that the EMPA analyses of plagioclase in Table 1 show considerable amounts of Na.

The plot of the octahedral composition in the MgAl-AlAl-FeAl ternary system (Güven, 1988) of both the

reaction products after three days and the VS smectite show the same degree of heterogeneity: the composition overlaps dioctahedral smectites from beidellite to Fe-rich montmorillonite. This result was also observed by Drief and Nieto (2000) for smectites from sedimentary environments. These authors related the fields of the ternary system to the specific origin of the smectite used to define them. The relationship between the octahedral cations of smectite shows that the substitutions of ^{VI}Al by Fe and Mg show a well-defined negative relationship (Figure 4). This may reflect the influence of the local parent chemistry in the composition of each smectite crystal.

Thus, different chemical factors control the formation of smectite in both natural and experimental en-
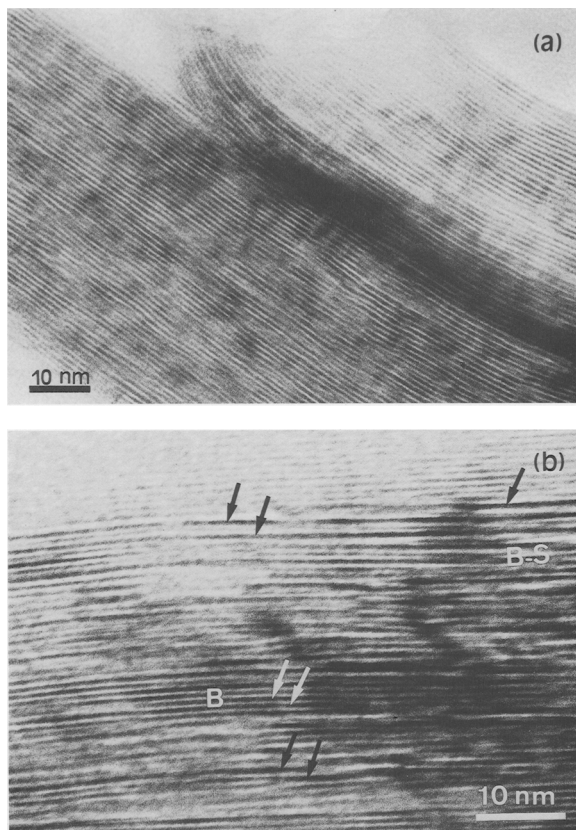
Figure 5. TEM images of clays formed after 14-d. a) lattice-fringe image of a well-crystallized smectite packet showing parallel layers with a 1.0-nm spacing. Some layers appear detached at the edge of the packet. b) random mixed-layer berthierine-smectite. White and black arrows show berthierine and smectite layers, respectively.

Table 3. AEM analyses for berthierine-rich B-S mixed-layer of 14-d reaction product normalized for 10 O and 8 (OH).

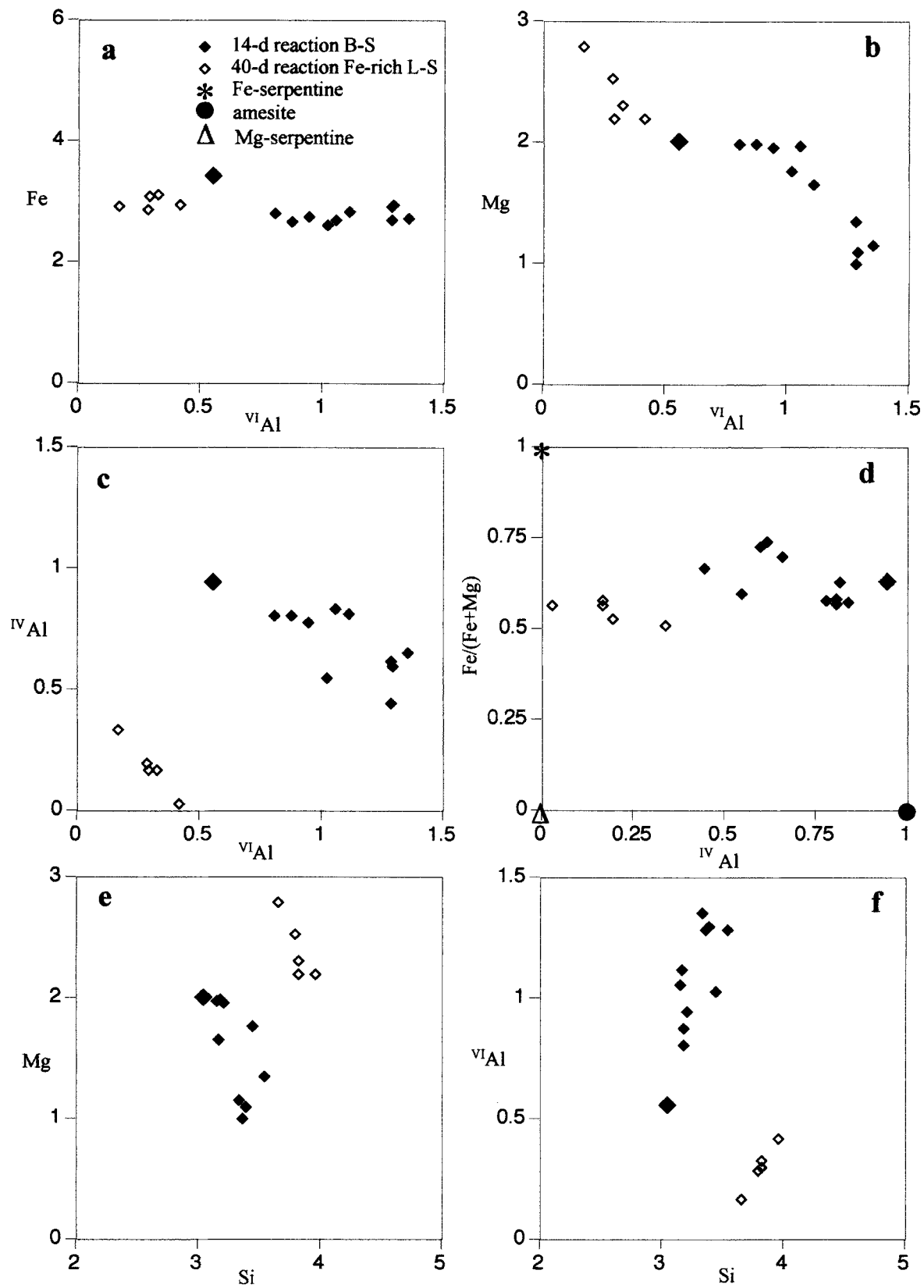|	Structural formulae of berthierine rich B-S mixed layer							
	Si	^{IV}Al	^{VI}Al	Fe	Mg	Σ oct. cat.	K	Ca
1	3.05	0.95	0.56	3.44	2.01	6.01	0.00	0.19
2	3.45	0.55	1.03	2.64	1.77	5.44	0.00	0.28
3	3.55	0.45	1.29	2.72	1.35	5.36	0.00	0.19
4	3.18	0.82	1.12	2.86	1.66	5.63	0.00	0.14
5	3.16	0.84	1.06	2.70	1.98	5.73	0.00	0.12
6	3.19	0.81	0.88	2.69	2.00	5.57	0.00	0.36
7	3.38	0.62	1.29	2.94	1.01	5.24	0.27	0.28
8	3.40	0.60	1.30	2.95	1.10	5.35	0.13	0.24
9	3.22	0.78	0.95	2.76	1.97	5.67	0.00	0.25
10	3.19	0.81	0.81	2.83	2.00	5.64	0.00	0.36
11	3.34	0.66	1.36	2.74	1.16	5.26	0.12	0.34

vironments. The intense alteration of plagioclase during its interaction with a high pH solution involves an initial ion exchange followed by diffusion through a depleted plagioclase surface composed mainly of Si and Al. As a result, a layer depleted in Ca and Na forms at the edges of plagioclase. Figure 7a depicts particles of smectite 100–200 nm in size detaching from plagioclase. Kawano and Tomita (1994) examined the growth of smectite from leached layers during the experimental alteration of plagioclase in deionized-distilled water at 150–225°C. They found that the leached layer increased successively in thickness and tended to detach from the albite surface as alteration proceeded to produce smectite.

The leaching of Na and Ca from plagioclase probably involved the formation of protocrystalline intermediate material such as that observed in Figure 9c (A'). Tazaki and Fyfe (1987) observed primitive clay precursors that formed on feldspar. Banfield and Eggleton (1990) found similar precursors on feldspar weathering products: protocrystalline material was considered as a probable intermediate precursor for

smectite. However, Banfield et al. (1991) found that the replacement of primary silicates (olivine, pyroxene, and feldspar) in the Albert volcanics resulted in the formation of smectite, but no persistent metastable intermediate phases in the reaction of primary silicates to smectites occurred. Ca- and Na-release probably destroyed the plagioclase structure during its interaction with the NaOH solution. The crystallization of smectite from the leached surface of plagioclase requires a change in the Al form (^{VI}Al in plagioclase to ^{IV}Al in smectite), a reorganization of tetrahedral and octahedral units, and the addition of hydroxyl groups and H_2O molecules from solution. The presence of weak lattice fringes in the protocrystalline material in Figure 9c probably reflects the initial stages of smectite recrystallization, consisting of the reconstruction of the basic 2:1 structure.

Smectite may also form by a dissolution-precipitation process. In this model, plagioclase releases Si and Al and ferromagnesian minerals, such as olivine and pyroxene. The latter minerals would release Mg and Fe necessary for the formation of smectite. However, the proportion of the cations in solution, in this case, is essential for the formation of smectite instead of other clay minerals. Smectites formed directly by precipitation from solution would contain high amounts of Mg and Fe since these two elements are readily released into solution. In fact, some analyses of smectite showed a high concentration of Fe and Mg in sample products of three days and in the VS smectites.

The formation of berthierine-smectite interstratifications

Berthierine is an uncommon mineral in soils. It usually develops in marine rocks or in sediments influenced by marine waters during early diagenesis. Although some studies describe berthierine from purely continental settings (e.g., Taylor, 1990), the occurrence is nonetheless rare in both marine and continental environments. This is probably related to the very special

Figure 8.   TEM micrograph showing smectite layers tightly intergrown with amorphous Fe oxyhydroxides. Black arrow points to Fe-rich amorphous material.
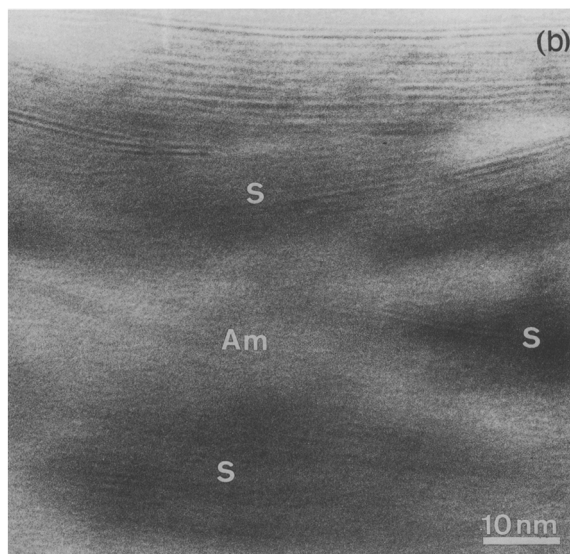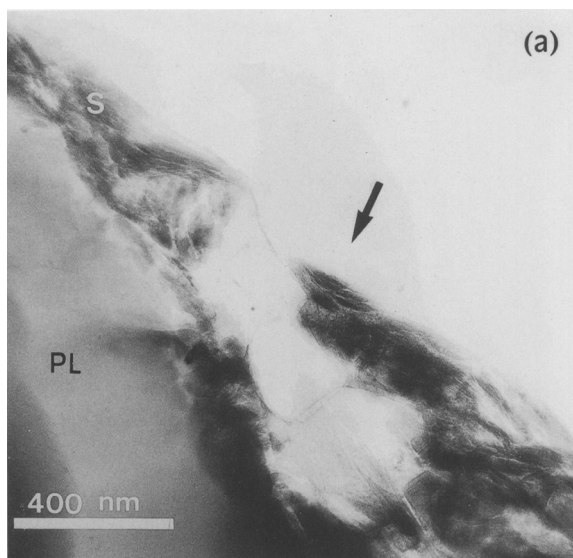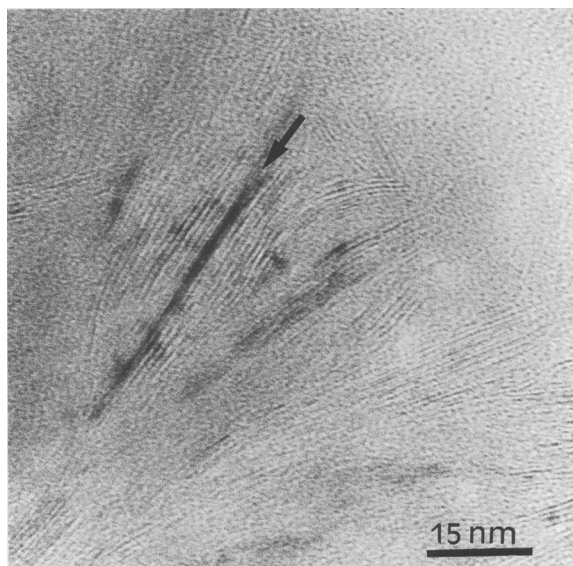

Figure 7.   a) Low magnification TEM image of smectites particles, associated with Fe-rich amorphous material, formed at the edge of plagioclase crystal. b) An enlarged image of the part shown by the black arrow in (a) showing smectite lattice fringes. In some cases the orientation of layers in the spindle-like smectite packets does not allow the visualization of lattice-fringes. S, PL, and Am designate smectite, plagioclase, and Fe-rich amorphous material, respectively.

conditions required during formation. The formation of berthierine in both natural and experimental studies requires very special conditions. Fritz and Toth (1997), in a study on the estimation of Eh, pH, and pCO_2 con-

ditions during the formation of Fe-rich berthierine from a Cretaceous laterite, suggested that the solution from which Fe-rich berthierine precipitates must: 1) be reducing; 2) have extremely low sulfate concentrations; 3) not be in contact with quartz; and 4) have a low $[Mg^{2+}]/[Fe^{2+}]$ ratio. These conditions are met in the present study, except where the $[Mg^{2+}]/[Fe^{2+}]$ ratio is not as low, as discussed by Fritz and Toth (1997). In contrast, however, Fritz and Toth consider Fe-rich berthierine, which differs chemically from the berthierine formed in this study.

The analyses in Table 3 were calculated on the basis of 14 O and 8 (OH). Although smectite generally dominated in the B-S interstratifications, the analyses presented in Table 3 were chosen in areas where berthierine layers were dominant to determine their chemical composition as closely as possible. Nevertheless, cations such as Ca and K, with no possible sites in the berthierine structure, were also found in the analyses (Table 3). These impurities resulted from variable quantities of smectite, as can be seen in Figure 5b. The analyses presented in Table 3 correspond to berthierine-rich B-S interstratifications. Moreover, some analyses showed a large number of octahedral vacancies and a high Si content. These results support the presence of smectite layers.

←

Figure 6.   Selected binary diagrams showing the compositional variation of the 14-d and 40-d reaction product. Note random interstratifications of berthierine-smectite and Fe-rich lizardite-smectite, respectively, using AEM analyses (see Tables 3 and 4). The large solid diamond indicates the closest analysis to end-member berthierine.
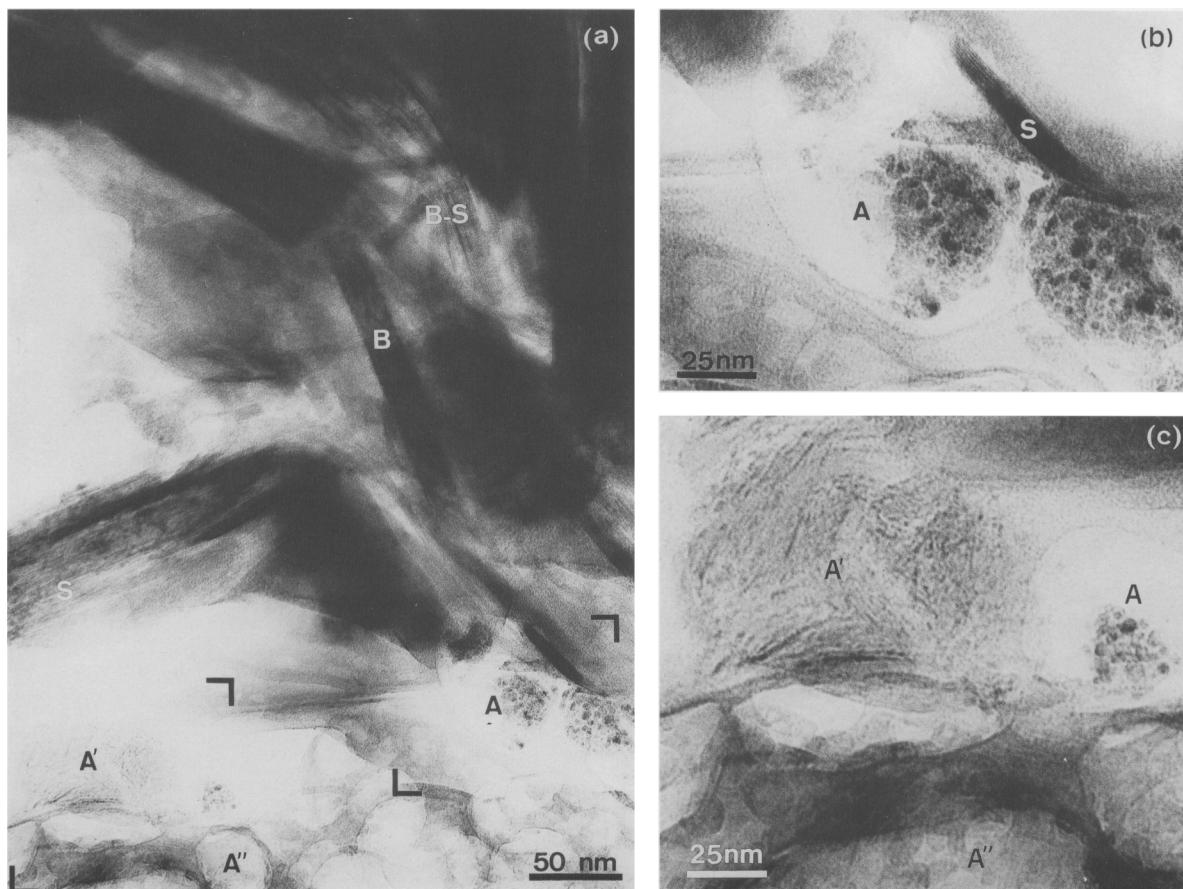
Figure 9. a) Low magnification TEM image of berthierine, smectite, and random interstratified B-S packets occurring together with diverse kinds of amorphous material formed after 14 d of reaction. b) Enlargement of the area situated at the bottom right of (a) showing curved smectite packets associated with Si-, Ca-, and Fe-rich amorphous material. c) Enlargement of the area situated at the bottom left of (a) showing details of three types of amorphous material. S = smectite, B = berthierine, B-S = random interstratified berthierine-smectite, A, A', and A" designate the three kinds of amorphous materials (see text for explanation).

The berthierine formed in the present study is similar to those reported in, for example James (1966), Brindley (1982), Li *et al.* (1997), and Abad-Ortega and Nieto (1995). The slight deviation of the chemical composition of the berthierine formed after 14 d of reaction from that of those reported in Figure 12 might be attributed to the intercalation of smectite.

Because berthierine occurs interstratified with smectite, it is clear that berthierine formed by the transformation of smectite. The layer-to-layer transformations were reported by several authors including: one biotite layer to one chlorite layer (Olives and Amouric, 1984; Olives, 1985), one smectite layer to one kaolinite layer (Amouric and Olives, 1998), and one serpentine layer to one illite layer (Amouric *et al.*, 1995). However, the S to B transformation could involve also the dissolution of smectite layers and a subsequent precipitation of berthierine, as has been argued for the neoformation of illite from smectite (*e.g.*, Leo Lunch *et al.*, 1997). The S to B transition

from a dioctahedral to a trioctahedral clay is related to the solution chemistry prevailing in the system. The plot of the chemical composition of B-S in the Si-Al-Fe + Mg ternary system (Figure 12) reveals that the transformation of smectite to B-S interstratification required the loss of Si and Al and a concomitant gain of Fe and Mg.

The main structural modification is the transformation of the structure from a 2:1 to 1:1 layer. The mechanism occurs at the unit-cell scale and preserves most of the pre-existing layers, although some parallel chemical changes are necessary for the transformation. This modification involves the removal of a tetrahedral sheet along with the adjacent interlayer region, to produce a decrease in volume. In addition, the remaining tetrahedral and octahedral sheets are modified, Si is replaced partially by Al in the tetrahedral sheet, Fe and Mg replace Al in the octahedral sheet, and H is added to the oxygen atoms of the 1:1 layer adjacent to the interlayer.
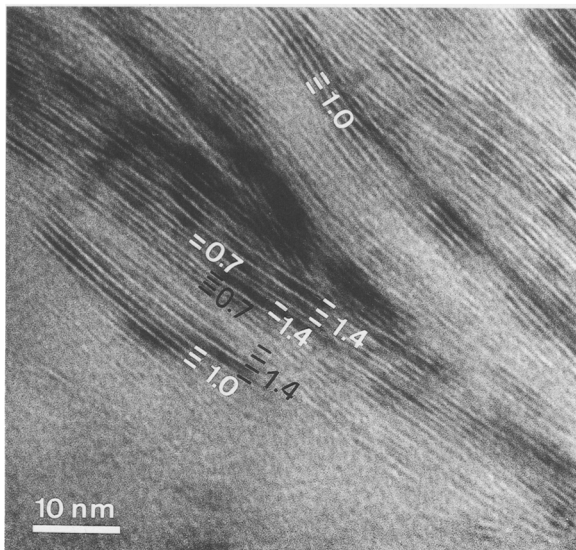
Figure 10.　TEM image of random mixed-layer Fe-rich L-S formed after 40 d of reaction. Layers with 1-nm spacing correspond to smectite and those with 0.7 and 1.4 nm to one and two-layer ferroan lizardite, respectively.

Table 4.　AEM analyses for Fe-rich L-S mixed-layer of 40-d reaction product normalized for 10 O and 8 (OH).

	Si	^{IV}Al	^{VI}Al	Fe	Mg	Σ oct. cat.	K	Ca
			Structural formulae of Fe-rich L-S mixed-layer					
1	3.97	0.03	0.42	2.97	2.21	5.60	0.05	0.18
2	3.83	0.17	0.33	3.13	2.32	5.78	0.00	0.14
3	3.80	0.20	0.29	2.89	2.53	5.71	0.00	0.25
4	3.66	0.34	0.17	2.93	2.80	5.89	0.00	0.20
5	3.83	0.17	0.30	3.11	2.21	5.63	0.04	0.29

No traces of berthierine were found in the subvolcanic-derived soil. The soil contains only smectite as a neoformed phase and some detrital minerals inherited from the parent rock (Drief and Nieto, 2000). The lack of berthierine in VS emphasizes the different conditions between natural and experimental environments. Several factors are responsible for controlling the formation of berthierine, with the most important being the pH and the amount of Fe and Mg in solution. The large supply of easily dissolved subvolcanic rock represents an abundant input of Fe and Mg. Under natural conditions, these elements can enter the solution leaving behind low Fe and Mg concentrations where smectite cannot transform to berthierine. However, in experimental conditions involving a closed system, the Fe and Mg remain. Furthermore, these elements can be incorporated into smectite layers which may lead to decomposition to berthierine. The effect of Fe on smectite is also observed in Figures 7b and 8. Another factor that is probably of great interest is the pH solution. Berthierine is known to be stable in high-pH solutions (Fritz and Toth, 1997). Thus, the formation of berthierine in the present study required a supply of Fe and Mg from ferromagnesian minerals such as pyroxenes, olivine, biotite, and amphibole and a reducing environment. Such conditions are not common in natural environments.

Amorphous material

In samples corresponding to reaction products after 14 and 40 d, the formation of metastable Fe-, Si-, Al-, and Ca-rich amorphous substances is favored by the high degree of saturation, which leads to irregular coordinations of ions, as well to the lower surface and strain energy of the spherical and ovoidal structures (Eggleton, 1987). In relation to the chemical composition of the observed amorphous phases, it is suggested that the first amorphous substances formed are especially rich in Fe, because the initial solution has a high Fe content released by the dissolution of ferromagnesians (pyroxenes and olivine). Analogously, be-
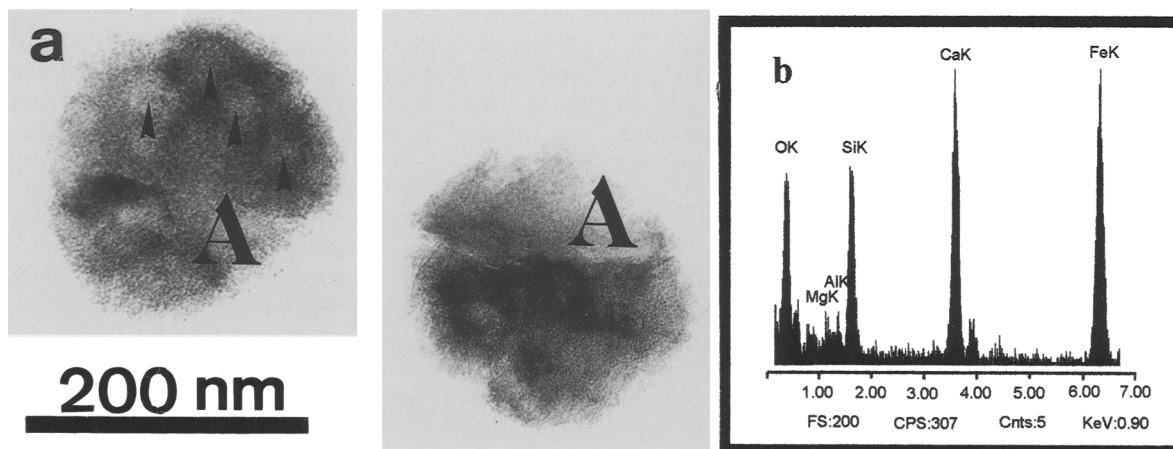

Figure 11.　a) Si-Ca-Fe amorphous material formed at 40 d of reaction showing a spheroidal-like morphology with minor rounded particles (arrows) within it. b) EDX spectrum of the rounded material.
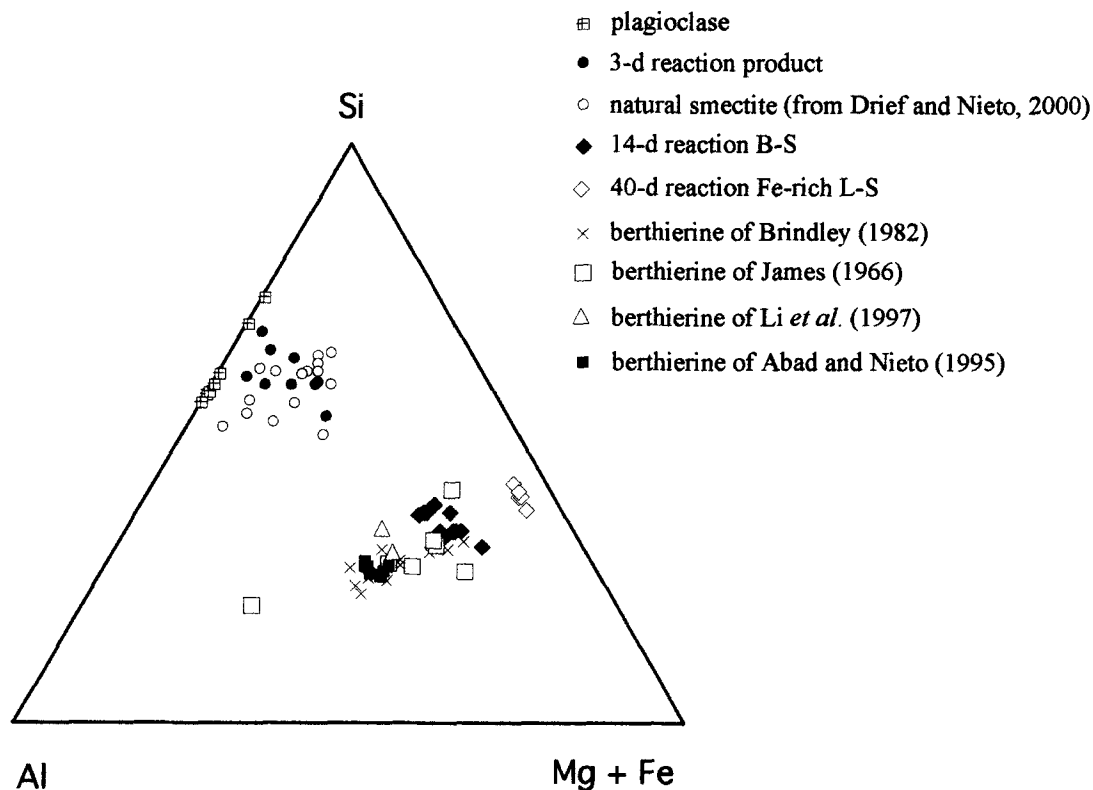
Figure 12. A synthetic plot in the Si-Al-(Fe + Mg) ternary system of the chemical composition of the starting plagioclase, clays formed in the present study along with VS smectite, and berthierine reported in the literature.

cause Ca is easily leached from plagioclase, Si-, Ca-, and Fe-rich amorphous substances are amply present in the 40-d reaction products, whereas other ions, such as Si and Al, remain a part of the structures of alu-minosilicates. The persistence of these amorphous metastable phases is favored by the slow reaction rates of the mineralogenetic process at low temperature (Berner, 1984).

Fe-rich lizardite-smectite interstratifications

The alteration process of the subvolcanic rock pro-duced Fe-rich L-S. Because the two phases, B-S and Fe-rich L-S interstratifications, are chemically well differentiated (see Figures 6 and 12), they are two dis-tinct phases. The chemical analyses shown in Table 4 are not consistent with berthierine because the Si con-tent in the tetrahedral sites is not typical of this min-eral. In a plot of Mg *vs.* Fe, such a composition falls between the greenalite and lizardite end-members. Al-though, Fe and Mg are always exchangeable cations, structural differences between these two end-members preclude the existence of a solid solution between them. The chemistry of the Fe-rich L-S is not suffi-ciently Fe-rich to be greenalite (Guggenheim *et al.,* 1982). Moreover, the *h0l* electron diffraction patterns of the Fe-rich L-S (not shown) are not consistent with

those of the modulated crystal structures of greenalite (Guggenheim and Eggleton, 1998). Therefore, the Fe-rich L-S found in the present study is an Fe-rich platy serpentine that should be referred to as "ferroan lizar-dite".

The ferroan lizardite and smectite (Fe-rich L-S) in-terstratifications showed a small decrease in the d val-ue (from 12.47 Å in the B-S interstratification to 12.33 Å in the Fe-rich L-S interstratification, in Figure 1). Table 4 shows the analyses corresponding to the Fe-rich L-S. The main differences between this phase and the B-S interstratification occur in the Si, Al, and Mg contents (Figure 6). In fact, the increase in Si in the tetrahedral sheet produced a decrease in Al (in both the tetrahedral and octahedral sheets) and a concomi-tant increase in Mg in the octahedral sheet, that is, the Tschermak vector. The stability of ferroan lizardite in-stead of berthierine after 40 d of reaction may be of importance in understanding the evolution of the sys-tem. Previous synthesis of iron-containing clay min-erals showed that reducing conditions are necessary and Fe^{2+} and Mg^{2+} are suitable for building a brucite-like layer (Harder, 1978). In the berthierine to ferroan lizardite transformation, the Tschermak substitution is favored by the progressive increase with time of the Si/Al ratio into the solution. Al is assumed to be the

more immobile cation and therefore the progress of the experiment would produce a solution depleted in Al in relation to the other cations, as usual in nature. Because of the precipitation of Si-, Ca-, and Fe-rich amorphous material as a sink for Fe, such substitutions involve Mg rather than Fe.

ACKNOWLEDGMENTS

REFERENCES

Abad-Ortega, M.M. and Nieto, F. (1995) Genetic and chemical relationships between berthierine, chlorite and cordierite in nodules associated to granitic pegmatites of Sierra Albarrana (Iberian Massif, Spain). *Contributions to Mineralogy and Petrology,* **120,** 327–336.

Ahn, J.H. and Peacor, D.R. (1985) Transmission electron microscopic study of diagenetic chlorite in Gulf Coast argillaceous sediments. *Clays and Clay Minerals,* **33,** 228–236.

Amouric, M., Gianetto, I., and Proust, D. (1988) 7, 10, and 14 Å mixed layer phyllosilicates studied structurally by TEM in pelitic rocks of the Piemontese zone (Venezuela). *Bulletin de Minéralogie,* **111,** 29–37.

Amouric, M. and Olives, J. (1998) Transformation mechanisms and interstratification in conversion of smectite to kaolinite: An HRTEM study. *Clays and Clay Minerals,* **46,** 521–527.

Amouric, M., Parron, C., Casalini, L., and Giresse, P. (1995) A (1:1) 7-Å Fe phase and its transformation in recent sediments: An HRTEM and AEM study. *Clays and Clay Minerals,* **43,** 446–454.

Bailey, S.W. (1980) Structures of layer silicates. In *Crystal Structure of Clay Minerals and Their X-ray Identification,* G.W. Brindley and G. Brown, eds., Mineralogical Society, London, 1–123.

Banfield, J.F. and Eggleton, R.A. (1990) Analytical transmission electron microscope studies of plagioclase, muscovite and feldspar weathering. *Clays and Clay Minerals,* **38,** 77–89.

Banfield, J.F., Jones, B.F., and Veblen, D.R. (1991) An AEM-TEM study of weathering and diagenesis, Albert Lake, Oregon: I. Weathering reactions in the volcanics. *Geochimica et Cosmochimica Acta,* **55,** 2781–2793.

Berner, R.A. (1984) Kinetics of weathering and diagenesis. In *Kinetics of Geochemical Processes, Reviews in Mineralogy, Volume 8,* A.C. Lasaga and R.J. Kirkpatrick, eds., Mineralogical Society of America, Washington, D.C., 111–134.

Bhattacharyya, D.P. (1983) Origin of berthierine in ironstones. *Clays and Clay Minerals,* **31,** 173–182.

Brindley, G.W. (1982) Chemical compositions of berthierines. A review. *Clays and Clay Minerals,* **30,** 153–155.

Christidis, G. (1989) Mineralogy, physical and chemical properties of deposits of Milos island, Greece. M.S. thesis, University of Hull, UK.

Drief, A. and Nieto, F. (2000) Chemical composition of smectites formed in clastic sediments. Implications for the smectite-illite transformation. *Clay Minerals,* **35,** 665–678.

Eggleton, R.A. (1987) Non-crystalline Fe-Si-Al-oxyhydroxides. *Clays and Clay Minerals,* **35,** 29–37.

Farmer, V.C., Krishnamurti, G.S.R., and Huang, P.M. (1991a) Synthetic allophane and layer-silicate formation in SiO_2-Al_2O_3-FeO-Fe_2O_3-MgO-H_2O systems at 23°C and 89°C in a calcareous environment. *Clays and Clay Minerals,* **39,** 561–570.

Farmer, V.C., McHardy, W.J., Palmieri, F., Violante, A., and Violante, P. (1991b) Synthetic allophane formed in calcareous environments: Nature, conditions of formation, and transformations. *Soil Science Society of America Journal,* **55,** 1162–1166.

Fritz, S.J. and Toth, T.A. (1997) An Fe-berthierine from a Cretaceous laterite: Part II. Estimation of Eh, pH and pCO_2 conditions of formation. *Clays and Clay Minerals,* **45,** 580–586.

Grauby, O., Petit, S., Decarreau, A., and Baronnet, A. (1993) The beidellite-saponite series: An experimental approach. *European Journal of Mineralogy,* **5,** 623–635.

Guggenheim, S. and Eggleton, R.A. (1998) Modulated crystal structures of greenalite and caryopilite: A system with long-range, in-plane structural disorder in the tetrahedral sheet. *The Canadian Mineralogist,* **36,** 163–179.

Guggenheim, S., Bailey, S.W., Eggleton, R.A., and Wilkes, P. (1982) Structural aspects of greenalite and related minerals. *The Canadian Mineralogist,* **20,** 1–18.

Güven, N. (1988) Smectite. In *Hydrous Phyllosilicates, Reviews in Mineralogy, Volume 19,* S.W. Bailey, ed., Mineralogical Society of America, Washington, D.C., 497–559.

Hallam, A. and Bradshaw, M.J. (1979) Bituminous shales and oolitic ironstones as indicators of transgressions and regressions. *Journal of the Geological Society of London,* **136,** 157–164.

Harder, H. (1978) Synthesis of iron layer silicate minerals under natural conditions. *Clays and Clay Minerals,* **26,** 65–72.

Hillier, S. and Velde, B. (1992) Chlorite interstratified with a 7Å mineral: An example from offshore Norway and possible implications for the interpretation of the composition of diagenetic chlorites. *Clay Minerals,* **27,** 475–486.

Jahren, J.S. and Aagaard, P. (1989) Compositional variation in diagenetic chlorites and illites, and relationship with formation-water chemistry. *Clay Minerals,* **24,** 157–170.

James, H.J. (1966) *Chemistry of the Iron-Rich Sedimentary Rocks.* U.S. Geological Survey Professional Paper 440-W, Washington, D.C., 59 pp.

Jiang, W.T., Peacor, D.R., and Slack, J.F. (1992) Microstructures, mixed layering, and polymorphism of chlorites and retrograde berthierine in the Kidd Creek Massive sulfide deposits, Ontario. *Clays and Clay Minerals,* **40,** 501–514.

Kawano, M. and Tomita, K. (1992) Formation of allophane and beidellite during hydrothermal alteration of volcanic glass below 200°C. *Clays and Clay Minerals,* **40,** 666–674.

Kawano, M. and Tomita, K. (1994) Growth of smectite from leached layer during experimental alteraction of albite. *Clays and Clay Minerals,* **42,** 7–17.

Kloprogge, J.T., Jansen, J.B.H., and Geus, J.W. (1990) Characterization of synthetic Na-beidellite. *Clays and Clay Minerals,* **38,** 409–414.

Lee, H.H. and Peacor, D.R. (1983) Interlayer transitions in phyllosilicates of Martinsburg shale. *Nature,* **303,** 608–609.

Leo Lunch, F., Makc, L.E., and Land, L.S. (1997) Burial diagenesis of illite/smectite in shales and the origins of authi-

genic quartz and secondary porosity in sandstones. *Geochimica et Cosmochimica Acta,* **61,** 1995–2006.

Li, G., Peacor, D.R., and Coombs, D.S. (1997) Transformation of smectite to illite in bentonite and associated sediments from Kaka Point, New Zealand: Contrast in rate and mechanism. *Clays and Clay Minerals,* **45,** 54–67.

Longstaffe, F.J., Racki, M.A., and Ayalon, A. (1992) Stable isotope studies of diagenesis in berthierine-bearing oil sands, Clearwater Formation, Alberta. In *Water Rock Interaction, Moderate and High Temperature Environments, Proceeding Seventh International Symposium on Water-Rock Interaction,* Y.K. Kharaka and A.S. Maest, eds., AA Balkema, Rotterdam, 955–958.

Lorimer, G.W. and Cliff, G. (1976) Analytical electron microscopy of minerals. In *Electron Microscopy in Mineralogy,* H.R. Wenk, ed., Springer-Verlag, New York, 506–519.

Morata, D., Puga, E., Demant, A., and Aguirre, L. (1997) Geochemistry and tectonic setting of the "ophites" from the External Zones of the Betic Cordilleras (S. Spain). *Estudios Geológicos,* **53,** 107–120.

Nickel, E.H. (1992) Solid-solutions in mineral nomenclature. *Canadian Mineralogist,* **30,** 231–234.

Olives, J. (1985) Biotites and chlorites as interlayered biotite-chlorite crystals. *Bulleltin de Minéralogie,* **108,** 635–641.

Olives, J. and Amouric, M. (1984) Biotite chloritization by interlayer brucitization as seen by HRTEM. *American Mineralogist,* **69,** 869–871.

Plee, D., Gatineau, L., and Fripiat, J.J. (1987) Pillaring processes of smectites with and without tetrahedral substitution. *Clays and Clay Minerals,* **35,** 81–88.

Portugal-Ferreira, M., Morata, D., Puga, E., Demant, A., and Aguirre, L. (1995) Evolución geoquímica y temporal del magmatismo básico Mesozoico en las Zonas Externas de las Cordilleras Béticas. *Estudios Geológicos,* **51,** 109–118.

Schiffman, P. and Southard, R.J. (1996) Cation exchange capacity of layer silicates and palagonitized glass in mafic volcanic rocks: A comparative study of bulk extraction and *in situ* techniques. *Clays and Clay Minerals,* **44,** 624–634.

Schultz, A., Stone, W.E.E., Poncelet, G., and Fripiat, J.J. (1987) Preparation and characterization of bidimensional zoolitic structures obtained from synthetic beidellite and hydroxy-aluminum solutions. *Clays and Clay Minerals,* **35,** 251–261.

Taylor, K.G. (1990) Berthierine from the non-marine Wealden (Early Cretaceous) sediments of south-east England. *Clay Minerals,* **25,** 391–399.

Tazaki, K. and Fyfe, W.S. (1987) Primitive clay precursors formed on feldspar. *Canadian Journal of Earth Sciences,* **24,** 506–527.

Toth, T.A. and Fritz, S.J. (1997) An Fe-berthierine from a Cretaceous laterite: Part I. Characterization. *Clays and Clay Minerals,* **45,** 564–579.